ACS Photonics

pubs.acs.org/journal/apchd5

Letter

Active Control of Multiple, Simultaneous Nonlinear Optical Processes in Plasmonic Nanogap Cavities

Qixin Shen, Weiliang Jin, Guoce Yang, Alejandro W. Rodriguez, and Maiken H. Mikkelsen*

Cite This: *ACS Photonics* 2020, 7, 901−907

Read Online

ACCESS | Metrics & More | Article Recommendations | Supporting Information

ABSTRACT: Plasmonic structures are promising to enhance and control nonlinear optical processes as the subwavelength-scale elements not only increase the local electric field intensities, but also result in relaxed phase matching conditions. This opens the possibility to observe and further manipulate multiple nonlinear optical processes simultaneously, which would be forbidden in bulk crystals due to incompatible phase matching requirements. Here we enhance and control the relative strength between third harmonic generation (THG), sum frequency generation (SFG), and four wave mixing (FWM) arising from 1 to 7 nm Al_2O_3 layers sandwiched between a gold film and silver nanorectangles. We demonstrate that the relative strength of the three, simultaneous nonlinear optical processes can be precisely controlled by either the ratio between the powers of the two excitations or the thickness of the Al_2O_3 layer. Furthermore, enhancements up to 10^6-fold for THG and FWM are observed along with 10^4-fold enhancements for SFG response when the resonance of the transverse and longitudinal mode of the cavity are matched to the two pump excitations. The ability to obtain and control multiple, nonlinear optical processes simultaneously open new capabilities for advanced on-chip manipulation and processing of optical signals on the deep nanoscale.

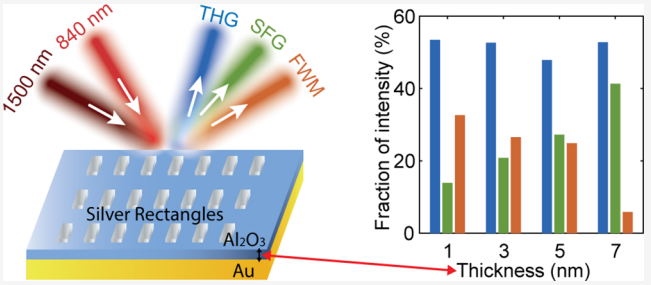

KEYWORDS: *plasmonics, nonlinear optics, metasurface, frequency conversion, tuning*

Plasmonic structures have attracted great interest as a means to investigate and enhance nonlinear optical processes[1] because of their subwavelength scale and ability to strongly localize and enhance electromagnetic fields. In particular, studies have focused on second harmonic generation (SHG)[2−7] and sum frequency generation (SFG),[8,9] which are second order nonlinear processes, as well as third harmonic generation (THG)[10−15] and four wave mixing (FWM),[16−20] which are third order nonlinear processes. In contrast to bulk crystals, the relaxation of phase matching conditions in plasmonic structures allows for the simultaneous observation of even and odd order nonlinear processes due to subwavelength dimensions.[1] Such observations have typically been achieved with a preferred combination of SHG and THG,[21−25] with limited investigations of other combinations such as SHG and FWM,[26] or THG and FWM.[27] Additionally, studies of 2D materials[28,29] and chemical imaging[30,31] report observations of up to three different nonlinear signals from a single sample; however, the different nonlinear processes are not observed simultaneously. A recent demonstration of an all-dielectric frequency mixer[32] is promising to obtain a variety of nonlinear responses across a broad spectral range, which relies on the large nonlinearities of constituent dielectric materials; however, questions still remain regarding the interplay between these nonlinear processes. To date, the interplay between multiple, simultaneous nonlinear processes has not been elucidated, which is critical to enable dynamic tuning and precise control of the relative strength of the processes. This would facilitate the precise manipulation of nonlinear responses at the nanoscale and is promising for on-chip functional nonlinear devices. Furthermore, plasmonic structures with dual spatially overlapped fundamental resonances to enhance nonlinear optical processes such as SFG and FWM, that require two distinct excitation wavelengths, have not been experimentally demonstrated.

Here, we employ a film-coupled nanorectangle plasmonic structure to observe THG, SFG, and FWM simultaneously. The relative strength of the three nonlinear processes can be controlled; either actively by manipulating the relative intensity of the two pump excitations or passively by varying the thickness of the dielectric Al_2O_3 layer. Additionally, the nonlinear responses are dramatically enhanced due to the high electromagnetic field intensities at both pump wave-

Received: January 4, 2020
Published: March 17, 2020

https://dx.doi.org/10.1021/acsphotonics.0c00011
ACS Photonics 2020, 7, 901−907

lengths due to the transverse and longitudinal modes of the nanogap plasmonic structure.

The plasmonic structures consist of an atomic layer deposited (ALD) Al_2O_3 film with a thickness of either 1, 3, 5, or 7 nm sandwiched between a 75 nm gold film and silver nanorectangles fabricated by electron-beam lithography (EBL), as shown in Figure 1a. The widths and lengths of the

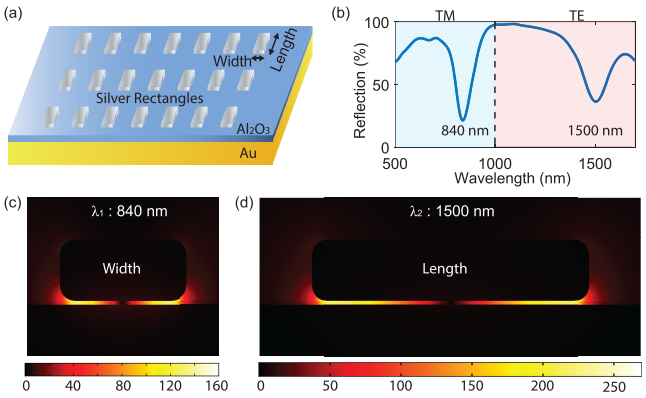

Figure 1. (a) Schematic of sample structure that consist of a 1 to 7 nm dielectric Al_2O_3 film sandwiched between 30 nm tall silver rectangles and a 75 nm gold film. (b) Measured reflection spectra from a sample with a 1 nm Al_2O_3 film embedded in the plasmonic nanogap structure. 500−1000 nm was measured for the transverse magnetic (TM) polarization, when the polarization of incident light is along rectangle width, and 1000−1700 nm was measured with the transverse electric (TE) polarization, when the polarization of incident light is along the rectangle length. (c) Simulated electric field enhancement distribution at 840 nm, where the resonance wavelength corresponds to the rectangle width. (d) Simulated electric field enhancement distribution at 1500 nm, where the resonance wavelength corresponds to the rectangle length.

nanorectangles were designed such that the resonance wavelengths from the transverse and longitudinal modes overlapped with the two excitation wavelengths $\lambda_{1(2)}$ = 840 (1500) nm, respectively. Reflectivity measurements were performed with white light, as shown in Figure 1b, where the two dips centered at the two excitation wavelengths represent the corresponding plasmon resonances from the nanorectangle. The 500−1000 nm spectral range was measured by a charge-coupled device (CCD) camera with the incident polarization parallel to the rectangle width and the 1000−1700 nm spectral range was measured by an InGaAs camera with the incident polarization parallel to the rectangle length. The electric field distribution is modified by the presence of the nanorectangle structures, giving rise to strongly localized and enhanced optical fields,[33−37] as seen in the simulations shown in Figure 1c,d performed by a finite-element method (COMSOL Multiphysics). The resonance wavelengths correspond to the width and length of the nanorectangles for TM and TE incident polarization, respectively.

Below, we briefly describe the main features associated with the three nonlinear processes explored in the experiment using two pumping frequencies ω_1 and ω_2. These processes include (i) surface SFG, which upconverts two photons at the pumping frequencies ω_1 and ω_2 to the summed frequency $\omega_S = \omega_1 + \omega_2$, (ii) THG, leading to an output photon at $\omega_T = 3\omega_2$, and (iii) degenerate FWM, leading to an output photon at $\omega_F = 2\omega_1 - \omega_2$. Our experimental observations, detailed below, show that the three nonlinear processes are significantly amplified due to resonant enhancement at the two pump frequencies. To qualitatively understand such processes, we applied coupled mode theory analysis in the nondepleted region,[38] detailed in the Supporting Information, to illustrate the scaling of the nonlinear power output with respect to the pumping power $P_{1(2)}$ and the pumping frequency detuning $\Delta\omega_{1(2)}$ from the respective resonant frequencies:

$$P^{\mathrm{SFG}} \propto P_1 P_2 \left[\frac{\gamma_{r1}}{\gamma_1^2 + \Delta\omega_1^2}\right]\left[\frac{\gamma_{r2}}{\gamma_2^2 + \Delta\omega_2^2}\right]$$

$$P^{\mathrm{THG}} \propto P_2^3 \left[\frac{\gamma_{r2}}{\gamma_2^2 + \Delta\omega_2^2}\right]^3$$

$$P^{\mathrm{FWM}} \propto P_1^2 P_2 \left[\frac{\gamma_{r1}}{\gamma_1^2 + \Delta\omega_1^2}\right]^2\left[\frac{\gamma_{r2}}{\gamma_2^2 + \Delta\omega_2^2}\right] \quad (1)$$

where we have assumed that there is a predominant mode around the resonance frequency $\omega_{1(2)}$. Here $\gamma_{i(ri)}$ denotes the total (radiative) decay rate of the mode at ω_i. Notably, the spectral function of the output power with respect to $\Delta\omega_{1(2)}$ can exhibit a high-order Lorentzian response.

Experimentally, the nonlinear signals were generated by two ~200 fs laser pulses with wavelengths at 840 and 1500 nm. Both excitation pulses were passed through the same objective and spatially overlapped on the sample. A delay stage was used to control the relative time difference between the two pulses, resulting in the emergence of three nonlinear signals near zero time delay as shown in Figure 2a. The signal centered at 500 nm is from THG and generated from the 1500 nm excitation. As the THG process does not involve the 840 nm excitation, the THG intensity remains constant as the time delay between the two pulses is varied. On the other hand, the remaining two nonlinear signals, which are from SFG and FWM, display a strong dependence on the time delay, reaching a maximum intensity at exactly the zero delay position. The red shift of the wavelength of the FWM response seen in Figure 2a is attributed to the approximately 10 nm spectral line width of the two excitations, resulting in the overlap of different peak wavelengths of the two excitation pulses at different time delays, also referred to as frequency chirping. A characteristic spectrum at zero time delay is shown in Figure 2b, which exhibits one peak arising from each of the nonlinear optical processes. To verify that the three peaks are indeed from the THG, SFG, and FWM processes described by eq 1, we performed power dependence measurements. Specifically, we measured the dependence of the nonlinear signals on the power of both excitation wavelengths by first varying one excitation power, and then the other, while keeping one excitation power constant. Figure 2c,d shows the intensities of the nonlinear signals as a function of the two excitation powers. Polynomial function fits by the power law exhibit good agreement with the experimental data, confirming the observed signals are indeed from the expected nonlinear optical processes in the undepleted region. Specifically, the THG response has a cubic power relation on the 1500 nm excitation power and remains constant with varying 840 nm excitation power. The SFG response increases linearly with increased 840 and 1500 nm excitation powers. The FWM response possesses a square power relation on the 840 nm excitation power and a linear relation on the 1500 nm excitation power.

https://dx.doi.org/10.1021/acsphotonics.0c00011
ACS Photonics 2020, 7, 901−907

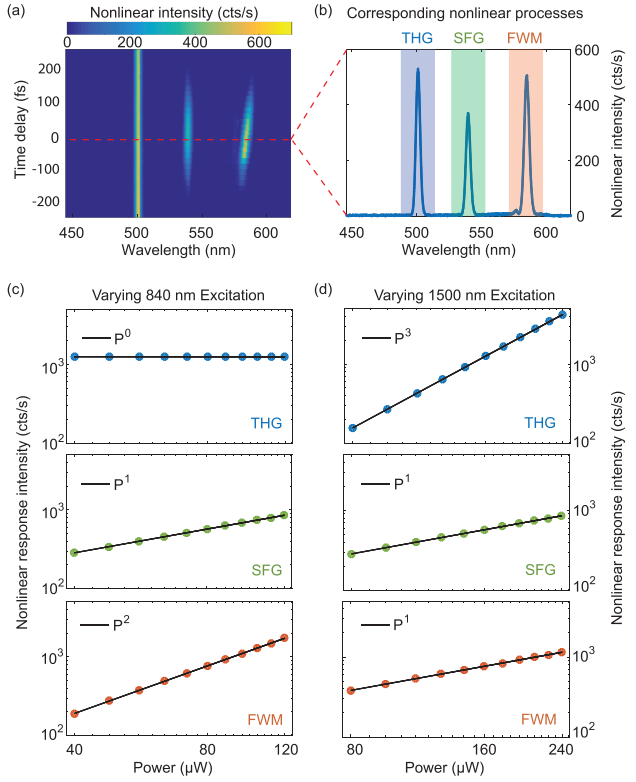

Figure 2. (a) Measured nonlinear response as a function of time delay between the two excitation pulses at 840 and 1500 nm. (b) Spectrum at zero time-delay, where three distinct peaks are observed simultaneously that arise from THG, SFG, and FWM. (c) Measured nonlinear signal as a function of 840 nm excitation power for the three nonlinear processes, as indicated in the figures. (d) Measured nonlinear signal as a function of 1500 nm excitation power for the three nonlinear processes, as indicated in the figures.

To take advantage of the enhanced electric field confined within the Al_2O_3 layer, the polarization of the two excitations are manipulated such that the 840 nm excitation is linearly polarized along the width of the nanorectangle and the 1500 nm excitation is linearly polarized along the length as shown in the schematic in Figure 3a. Additionally, excitation wavelength

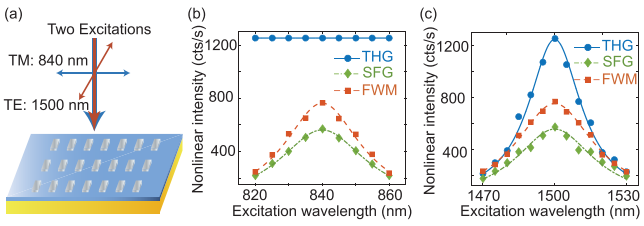

Figure 3. (a) Illustration of the experimental geometry, where the blue arrow represents 840 nm excitation with TM polarization (excitation polarization along rectangle width) and the red arrow represents 1500 nm excitation with TE polarization (excitation polarization along rectangle length). (b) THG (blue), SFG (green), and FWM (orange) intensity as the excitation wavelength is varied from 820 to 860 nm for a 1 nm Al_2O_3 film embedded in the plasmonic nanogap structure. (c) THG (blue), SFG (green), and FWM (orange) intensity as the excitation wavelength is varied from 1470 to 1530 nm for a 1 nm Al_2O_3 film embedded in the plasmonic nanogap structure. Data points are experimental results and curves are Lorentzian function fits to the data.

dependence measurements were performed to verify the importance of spectrally matching the plasmon resonance with the excitation wavelength. Figure 3b,c shows the characteristic results from a 1 nm Al_2O_3 dielectric layer embedded between a gold ground plane and silver nanorectangles, with the shorter wavelength excitation at 80 μW and the longer wavelength excitation at 160 μW. The width and length of the nanorectangle are selected such that the resonances from the transverse and longitudinal modes are centered at 840 and 1500 nm, respectively (Figure 1b). When one excitation is detuned from the resonance at 840 nm, while the other excitation remains constant at 1500 nm, the SFG and FWM intensities decrease dramatically because of the reduced electric field intensity in the nonlinear media, as the plasmonic structure is off-resonance with the excitation. There is no variation in the THG intensities since this process only relies on the 1500 nm excitation. Similarly, when the other excitation wavelength is detuned from the resonance at 1500 nm, while the 840 nm excitation remains constant, the THG, SFG, and FWM intensities decrease dramatically. However, the rate of the decrease in the nonlinear signal with detuning of the excitation wavelengths varies for the different nonlinear processes, as seen in Figure 3b,c. This variation can be explained by the different-order Lorentzian line shapes, as described by eq 1, which means that different nonlinear processes have different behaviors in terms of their full width at half-maximum (fwhm) as the excitation wavelengths are detuned from the resonance.

Next, we investigate the effect of the thickness of the Al_2O_3 layer on the enhancement of the nonlinear response and the fwhm of the excitation wavelength dependence. To this end, four different thicknesses (1, 3, 5, and 7 nm) were fabricated by ALD. The enhancement of the nonlinear response is defined as the nonlinear response from the Al_2O_3 embedded between the silver nanorectangles and the gold film divided by the nonlinear response from the control sample consisting of Al_2O_3 layer on the gold film (without the silver nanorectangles) under the same excitation conditions. The Al_2O_3 layer on the gold film is selected as the control sample since the nonlinear intensity from a sub-7 nm Al_2O_3 layer itself is too weak to detect. The intensity of the nonlinear response from the Al_2O_3 layer on gold remains constant for different Al_2O_3 layer thicknesses, with the exception of the SFG intensity, which increases slightly for thicker layers (detailed spectra in Supporting Information). However, the SFG intensity remains within the same order of magnitude for all Al_2O_3 layer thicknesses which makes it reasonable to calculate the enhancement factor using these reference intensities. It should be noted that different excitation powers were employed for the control sample and plasmonic nanogap structures in order to prevent damage of the silver nanorectangles from the strongly enhanced electric fields in the nanogaps. Therefore, the power laws shown in Figure 2c,d were used to extrapolate the nonlinear intensities taken at different excitation powers to the same condition. As summarized in Figure 4a, the nonlinear optical processes experience dramatic enhancements in the presence of the plasmonic nanogap structures as compared to only the gold film. In particular, a greater enhancement in the nonlinear signals are observed for thinner Al_2O_3 layers due to the higher electric field intensities in the gap region for smaller nanogap structures. This indicates that the effect of the enhanced electric field induced by the plasmonic structure dominates the enhancement as opposed to the total thickness

https://dx.doi.org/10.1021/acsphotonics.0c00011
ACS Photonics 2020, 7, 901−907

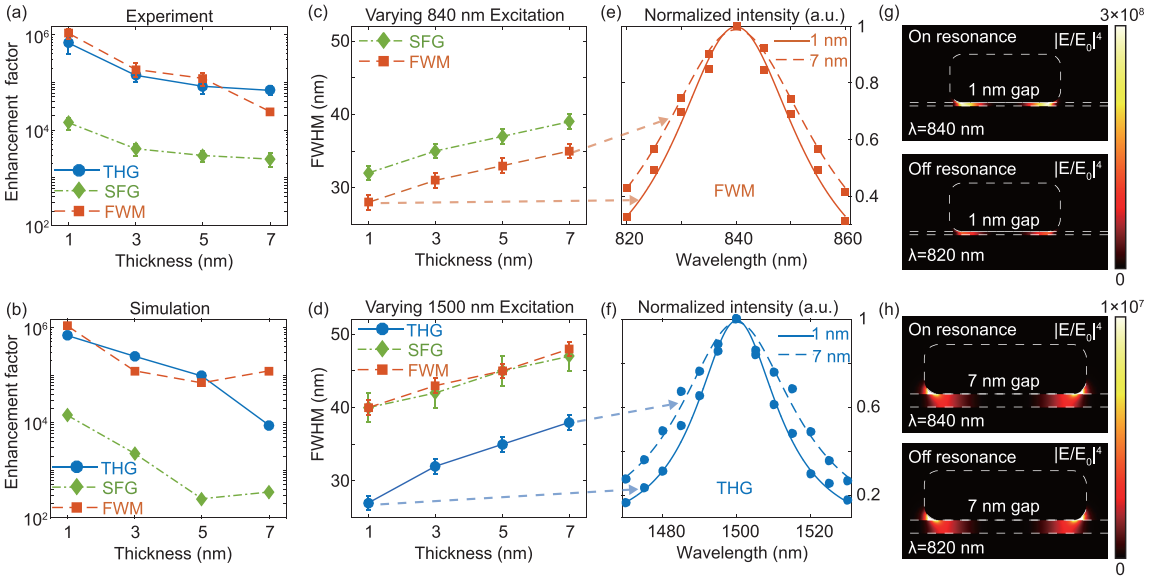

Figure 4. (a, b) Enhancement of the nonlinear signal for the three different nonlinear optical processes and for four different Al_2O_3 thicknesses ranging from 1 to 7 nm. The enhancement factor is defined as the nonlinear signal of the Al_2O_3 film embedded in the plasmonic nanogap structure divided by the nonlinear signal from an Al_2O_3 film of the same thickness on gold and under the same excitation conditions: (a) experiment; (b) simulation. The enhancement factor at 1 nm is normalized to the experimental value for easier comparison. (c, d) Fwhm of the excitation wavelength dependence, where the two excitation wavelengths are varied independently: (c) 840 nm excitation is varied; (d) 1500 nm excitation is varied. Data points with error bars are from five experimental measurements taken at different areas on each sample. Lines serve as a guide to the eye. (e, f) Normalized nonlinear intensity as a function of excitation wavelength from which the fwhm shown in (c) and (d) are obtained. The arrows represent the corresponding nonlinear optical process and gap thickness. (g, h) Biquadratic electric field enhancement distribution $|\boldsymbol{E}/\boldsymbol{E}_0|^4$, when the structure is on and off resonance with the excitation: (g) 1 nm Al_2O_3 gap; (h) 7 nm Al_2O_3 gap.

of nonlinear media in the gap region. From Figure 4a, it is also observed that the enhancement factors of THG and FWM processes are very similar and on the same order of magnitude for all four studied thicknesses and between 10× and 76× larger than the enhancement observed for SFG depending on the Al_2O_3 thickness. This difference in enhancement arises as THG and FWM are third order nonlinear processes, resulting in the generation of a nonlinear signal with a cubic power dependence on the excitation electric field intensity, while SFG is a second order nonlinear process with a square power law relation. Thus, a larger enhancement is expected for higher-order nonlinear processes, which is also observed experimentally here. This is further highlighted by the observation that the square of the enhancement factors of the THG and FWM responses are approximately the same as the cube of the enhancement factor of the SFG response, which are close to 10^{12} for the 1 nm gap as an example. The maximum efficiencies for these nonlinear processes are extracted using a calibrated light source and estimated to be 7.44×10^{-4}%, 8.55×10^{-6}%, and 1.28×10^{-3}% for THG, SFG, and FWM, respectively, from the 1 nm Al_2O_3 layer embedded in the plasmonic structures. We also numerically investigate the impact of the Al_2O_3 thickness on the resulting nonlinear generation, which is detailed in the Supporting Information and summarized in Figure 4b. The simulated enhancement factor is normalized to the experimental value at 1 nm for easier comparison of the dependence on gap thickness. For both FWM and THG processes, qualitative agreement between the numerical and the experimental results can be observed for thicknesses smaller than 7 nm. As for the SFG process, the numerical results suggest a more pronounced thickness dependence, which may be attributed to nonlocal optical responses such as the anomalous skin effect in metals.[39] Thus, the actual effective material loss on the surface, particularly relevant in SFG processes, might be strongly underestimated in our simulation which relies on a local material response model.

In addition to the enhancement factor, the thickness of the Al_2O_3 gap layer also affects the fwhm of the nonlinear intensity as a function of excitation wavelength in cases where the plasmonic structure is off-resonance with the excitation wavelength. The fwhm of the excitation wavelength dependence is depicted in Figure 4c and d for different thicknesses of the Al_2O_3 layer and for the various nonlinear optical processes. The error bars indicate the standard deviation from five independent measurements on different areas of the same sample and are much smaller than variations between samples with different thicknesses of the Al_2O_3 layer. Figure 4e,f shows the representative excitation wavelength dependence spectra from which the data in Figure 4c,d are extracted. From these spectra, it is observed that the fwhm exhibits a clear dependence on the thickness of the Al_2O_3 layer and the particular nonlinear optical process being generated. First, it is observed experimentally that the fwhm of the excitation wavelength dependence increases for larger Al_2O_3 thicknesses. This can be qualitatively understood based on the decrease in the electric field amplitude between on and off resonant excitation for 1 and 7 nm gaps, which as seen in Figure 4g,h is more dramatic for the smaller gap size. Second, it is observed that the fwhm of the excitation wavelength dependence varies with different nonlinear optical processes, as shown in Figure 4c,d. This is expected from eq 1, which illustrates that the spectral response as a function of excitation frequency exhibits a higher-order Lorentzian line shape and, consequently, a narrower fwhm, for higher-order power relations of the nonlinear intensity versus excitation power. Thus, for higher order power dependence, the amplitude of the nonlinear

https://dx.doi.org/10.1021/acsphotonics.0c00011
ACS Photonics 2020, 7, 901−907

polarization decreases more rapidly with decreased electric field intensity as the excitation moves away from the resonance wavelength of the plasmonic structures, resulting in smaller fwhm. Specifically, the fwhm of THG response when varying the 1500 nm excitation is smaller than SFG and FWM due to its cubic dependence (third-order Lorentzian line shape) on the excitation power compared with the linear dependence of SFG and FWM (simple Lorentzian line shape).

Finally, we investigate control of the relative strength of the three, simultaneously occurring nonlinear processes: first, passively by varying the thickness of the Al_2O_3 layer and, next, actively by varying the excitation power ratio between the 840 and 1500 nm excitations. To demonstrate passive control, the same excitation conditions (840 nm excitation: 140 μW, 1500 nm excitation: 280 μW) were employed on four samples with different Al_2O_3 layer thicknesses embedded in the nanogap structures. The fraction of one nonlinear intensity is defined as its intensity divided by the sum of all three nonlinear intensities. It is observed in Figure 5a that the fraction of THG

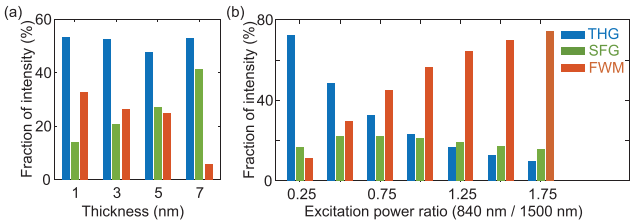

Figure 5. (a) Tunability of the relative strength of the three simultaneously occurring nonlinear processes for different thicknesses of the Al_2O_3 film. For these measurements, the 840 nm excitation power is 140 μW and the 1500 nm excitation power is 280 μW. (b) Active tuning of the relative strength of the three nonlinear processes by varying the power ratio between the 840 and 1500 nm excitation measured from the 1 nm sample. For these measurements, the 1500 nm excitation power is 160 μW and the 840 nm excitation power is varied from 40 to 280 μW with the corresponding power ratio shown in the figure.

intensity remains constant with increasing thickness, while the fraction of SFG intensity increases and the fraction of FWM intensity decreases. It should be noted that the fractions of nonlinear intensities as a function of dielectric thickness may be different for different excitation power conditions, which provides active tuning in addition to passive tuning from the variation of gap thickness. Next, to demonstrate active control, experimental results are shown in Figure 5b, where the 1500 nm excitation power is constant at 160 μW, while the 840 nm excitation power varies, giving a power ratio in the range of 0.25 to 1.75. With a larger excitation power ratio, the THG intensity remains constant since it only depends on the excitation power at 1500 nm. On the other hand, the SFG and FWM intensities increase since they are linearly and squarely proportional to the 840 nm excitation power, respectively. It is observed that the FWM intensity increases more rapidly than the SFG intensity, which is due to the second order power relation for FWM compared to the linear power relation for SFG. As a result, the fraction of THG intensity decreases for higher excitation power ratios as the other two nonlinear intensities increase dramatically.

In conclusion, enhancement factors approaching 10^6-fold for THG and FWM and 10^4-fold for SFG were observed experimentally from plasmonic nanogap cavities. Three nonlinear optical processes, THG, FWM, and SFG, were generated simultaneously and their relative strength was controlled actively by varying the ratio of the power between the two excitations and passively by varying the thickness of the Al_2O_3 gap layer. The capability to precisely control the interplay between these simultaneous nonlinear signals may facilitate applications such as on-chip nonlinear devices as well as provide new insights into nonlinear generation at the deep nanoscale. Nanorectangle structures were fabricated such that both the transverse and the longitudinal mode contribute to the enhanced electric field intensities confined within the nanogap structure at two distinct wavelengths, thus significantly increasing the generated nonlinear signal. The enhancement of the relative strength of these nonlinear signals is important for future applications where a local weak pump is more important than overall conversion efficiency such as for local generation of extreme ultraviolet (EUV) light or four photon luminescence for near-field lithography. The fwhm of the generated nonlinear signals were measured as a function of the excitation wavelength for different Al_2O_3 thicknesses, which indicates that the observed enhancement of the nonlinear signal is mainly due to the strongly enhanced electric field confined within the dielectric Al_2O_3 layer itself and not the surrounding plasmonic structure. It is observed that the generated nonlinear signal increase with thinner Al_2O_3 gap layers, which is consistent with numerical simulations and offers design principles to utilize ultrathin dielectric materials for future efficient nanoscale nonlinear devices. Additionally, the nonlinear coefficient of the Al_2O_3 used in these studies is very small compared with other common nonlinear materials,[40] providing a pathway to further increase the generated nonlinear signal by employing other dielectric materials with larger nonlinear coefficients. The ability to observe different orders of nonlinear optical processes and tune their relative strength provides a pathway to utilize multiple, simultaneous nonlinear optical processes and may find applications in, for example, optical frequency mixers and quantum information.

■ ASSOCIATED CONTENT

Supporting Information

The Supporting Information is available free of charge at https://pubs.acs.org/doi/10.1021/acsphotonics.0c00011.

Additional details on the fabrication method, optical setup, control measurements, theoretical analysis, and simulation method (PDF)

■ AUTHOR INFORMATION

Corresponding Author

Maiken H. Mikkelsen − *Department of Electrical and Computer Engineering, Duke University, Durham, North Carolina 27708, United States;* orcid.org/0000-0002-0487-7585; Phone: +1 (919) 660-0185; Email: m.mikkelsen@duke.edu

Authors

Qixin Shen − *Department of Physics, Duke University, Durham, North Carolina 27708, United States*

Weiliang Jin − *Department of Electrical Engineering, Princeton University, Princeton, New Jersey 08544, United States*

Guoce Yang − *Department of Electrical and Computer Engineering, Duke University, Durham, North Carolina 27708, United States; State Key Laboratory of Precision Measurement*

https://dx.doi.org/10.1021/acsphotonics.0c00011
ACS Photonics 2020, 7, 901−907

Technology and Instruments, Department of Precision Instrument, Tsinghua University, Beijing 100084, China; orcid.org/0000-0002-6566-7776

Alejandro W. Rodriguez − *Department of Electrical Engineering, Princeton University, Princeton, New Jersey 08544, United States*

Complete contact information is available at: https://pubs.acs.org/10.1021/acsphotonics.0c00011

Notes

The authors declare no competing financial interest.

■ ACKNOWLEDGMENTS

This work was supported by the National Science Foundation (NSF) Grant Number EFMA-1640986. Q.S. and M.H.M. also acknowledge support from the Army Research Office (ARO) Grant Number W911NF1610471. W.J. and A.W.R. also acknowledge support from the NSF Grant Numbers DMR-1454836, DMR 1420541 and the Cornell Center for Materials Research MRSEC award no. DMR1719875.

■ REFERENCES

(1) Kauranen, M.; Zayats, A. V. Nonlinear Plasmonics. *Nat. Photonics* **2012**, *6* (11), 737−748.
(2) Walsh, G. F.; Dal Negro, L. Enhanced Second Harmonic Generation by Photonic-Plasmonic Fano-Type Coupling in Nanoplasmonic Arrays. *Nano Lett.* **2013**, *13* (7), 3111−3117.
(3) Thyagarajan, K.; Rivier, S.; Lovera, A.; Martin, O. J. F. Enhanced Second-Harmonic Generation from Double Resonant Plasmonic Antennae. *Opt. Express* **2012**, *20* (12), 12860.
(4) Butet, J.; Brevet, P.-F.; Martin, O. J. F. Optical Second Harmonic Generation in Plasmonic Nanostructures: From Fundamental Principles to Advanced Applications. *ACS Nano* **2015**, *9* (11), 10545−10562.
(5) Celebrano, M.; Wu, X.; Baselli, M.; Großmann, S.; Biagioni, P.; Locatelli, A.; De Angelis, C.; Cerullo, G.; Osellame, R.; Hecht, B.; et al. Mode Matching in Multiresonant Plasmonic Nanoantennas for Enhanced Second Harmonic Generation. *Nat. Nanotechnol.* **2015**, *10* (5), 412−417.
(6) Thyagarajan, K.; Butet, J.; Martin, O. J. F. Augmenting Second Harmonic Generation Using Fano Resonances in Plasmonic Systems. *Nano Lett.* **2013**, *13* (4), 1847−1851.
(7) Zhang, Y.; Grady, N. K.; Ayala-Orozco, C.; Halas, N. J. Three-Dimensional Nanostructures as Highly Efficient Generators of Second Harmonic Light. *Nano Lett.* **2011**, *11* (12), 5519−5523.
(8) Bai, S.; Fang, M.; Sha, W. E. I.; Qu, Y.; Jin, Z.; Tian, J.; Du, K.; Yu, S.; Qiu, C. W.; Qiu, M.; et al. Chip-Scale Plasmonic Sum Frequency Generation. *IEEE Photonics J.* **2017**, *9* (3), 1−8.
(9) Lis, D.; Caudano, Y.; Henry, M.; Demoustier-Champagne, S.; Ferain, E.; Cecchet, F. Selective Plasmonic Platforms Based on Nanopillars to Enhance Vibrational Sum-Frequency Generation Spectroscopy. *Adv. Opt. Mater.* **2013**, *1* (3), 244−255.
(10) Shen, Q.; Hoang, T. B.; Yang, G.; Wheeler, V. D.; Mikkelsen, M. H. Probing the Origin of Highly-Efficient Third-Harmonic Generation in Plasmonic Nanogaps. *Opt. Express* **2018**, *26* (16), 20718−20725.
(11) Lassiter, J. B.; Chen, X.; Liu, X.; Ciracì, C.; Hoang, T. B.; Larouche, S.; Oh, S. H.; Mikkelsen, M. H.; Smith, D. R. Third-Harmonic Generation Enhancement by Film-Coupled Plasmonic Stripe Resonators. *ACS Photonics* **2014**, *1* (11), 1212−1217.
(12) Aouani, H.; Rahmani, M.; Navarro-Cía, M.; Maier, S. A. Third-Harmonic-Upconversion Enhancement from a Single Semiconductor Nanoparticle Coupled to a Plasmonic Antenna. *Nat. Nanotechnol.* **2014**, *9* (4), 290−294.
(13) Grinblat, G.; Li, Y.; Nielsen, M. P.; Oulton, R. F.; Maier, S. A. Enhanced Third Harmonic Generation in Single Germanium Nanodisks Excited at the Anapole Mode. *Nano Lett.* **2016**, *16* (7), 4635−4640.
(14) Shcherbakov, M. R.; Neshev, D. N.; Hopkins, B.; Shorokhov, A. S.; Staude, I.; Melik-Gaykazyan, E. V.; Decker, M.; Ezhov, A. A.; Miroshnichenko, A. E.; Brener, I.; et al. Enhanced Third-Harmonic Generation in Silicon Nanoparticles Driven by Magnetic Response. *Nano Lett.* **2014**, *14* (11), 6488−6492.
(15) Metzger, B.; Hentschel, M.; Schumacher, T.; Lippitz, M.; Ye, X.; Murray, C. B.; Knabe, B.; Buse, K.; Giessen, H. Doubling the Efficiency of Third Harmonic Generation by Positioning. *Nano Lett.* **2014**, *14*, 2867−2872.
(16) Kravtsov, V.; Ulbricht, R.; Atkin, J. M.; Raschke, M. B. Plasmonic Nanofocused Four-Wave Mixing for Femtosecond near-Field Imaging. *Nat. Nanotechnol.* **2016**, *11* (5), 459−464.
(17) Li, G.; Sartorello, G.; Chen, S.; Nicholls, L. H.; Li, K. F.; Zentgraf, T.; Zhang, S.; Zayats, A. V. Spin and Geometric Phase Control Four-Wave Mixing from Metasurfaces. *Laser Photonics Rev.* **2018**, *12* (6), 1−6.
(18) Zhang, Y.; Wen, F.; Zhen, Y.-R.; Nordlander, P.; Halas, N. J. Coherent Fano Resonances in a Plasmonic Nanocluster Enhance Optical Four-Wave Mixing. *Proc. Natl. Acad. Sci. U. S. A.* **2013**, *110* (23), 9215−9219.
(19) Almeida, E.; Prior, Y. Rational Design of Metallic Nanocavities for Resonantly Enhanced Four-Wave Mixing. *Sci. Rep.* **2015**, *5*, 1−10.
(20) Genevet, P.; Tetienne, J. P.; Gatzogiannis, E.; Blanchard, R.; Kats, M. A.; Scully, M. O.; Capasso, F. Large Enhancement of Nonlinear Optical Phenomena by Plasmonic Nanocavity Gratings. *Nano Lett.* **2010**, *10* (12), 4880−4883.
(21) Scalora, M.; Vincenti, M. A.; De Ceglia, D.; Roppo, V.; Centini, M.; Akozbek, N.; Bloemer, M. J. Second- and Third-Harmonic Generation in Metal-Based Structures. *Phys. Rev. A: At., Mol., Opt. Phys.* **2010**, *82* (4), 1−14.
(22) Klein, M. W.; Wegener, M.; Feth, N.-A.; Linden, S. Experiments on Second- and Third-Harmonic Generation from Magnetic Metamaterials: Erratum. *Opt. Express* **2008**, *16* (11), 8055.
(23) Levy, U.; Silberberg, Y. Second and Third Harmonic Waves Excited by Focused Gaussian Beams. *Opt. Express* **2015**, *23* (21), 27795.
(24) Sartorello, G.; Olivier, N.; Zhang, J.; Yue, W.; Gosztola, D. J.; Wiederrecht, G. P.; Wurtz, G.; Zayats, A. V. Ultrafast Optical Modulation of Second- and Third-Harmonic Generation from Cut-Disk-Based Metasurfaces. *ACS Photonics* **2016**, *3* (8), 1517−1522.
(25) Sajedian, I.; Zakery, A.; Rho, J. High Efficiency Second and Third Harmonic Generation from Magnetic Metamaterials by Using a Grating. *Opt. Commun.* **2017**, *397* (February), 17−21.
(26) Xue, X.; Leo, F.; Xuan, Y.; Jaramillo-Villegas, J. A.; Wang, P. H.; Leaird, D. E.; Erkintalo, M.; Qi, M.; Weiner, A. M. Second-Harmonic-Assisted Four-Wave Mixing in Chip-Based Microresonator Frequency Comb Generation. *Light: Sci. Appl.* **2017**, *6* (4), 1−10.
(27) Chen-Jinnai, A.; Kato, T.; Fujii, S.; Nagano, T.; Kobatake, T.; Tanabe, T. Broad Bandwidth Third-Harmonic Generation via Four-Wave Mixing and Stimulated Raman Scattering in a Microcavity. *Opt. Express* **2016**, *24* (23), 26322−26331.
(28) Zhang, J.; Ye, M.; Bhandari, S.; Muqri, A. K. M.; Long, F.; Bigham, S.; Yap, Y. K.; Suh, J. Y. Enhanced Second and Third Harmonic Generations of Vertical and Planar Spiral MoS_2 Nanosheets. *Nanotechnology* **2017**, *28* (29), 295301.
(29) Säynätjoki, A.; Karvonen, L.; Rostami, H.; Autere, A.; Mehravar, S.; Lombardo, A.; Norwood, R. A.; Hasan, T.; Peyghambarian, N.; Lipsanen, H.; et al. Ultra-Strong Nonlinear Optical Processes and Trigonal Warping in MoS_2 layers. *Nat. Commun.* **2017**, *8* (1), 1−8.
(30) Schaller, R. D.; Johnson, J. C.; Wilson, K. R.; Lee, L. F.; Haber, L. H.; Saykally, R. J. Nonlinear Chemical Imaging Nanomicroscopy: From Second and Third Harmonic Generation to Multiplex (Broad-Bandwidth) Sum Frequency Generation near-Field Scanning Optical Microscopy. *J. Phys. Chem. B* **2002**, *106* (20), 5143−5154.
(31) Selm, R.; Krauss, G.; Leitenstorfer, A.; Zumbusch, A. Simultaneous Second-Harmonic Generation, Third-Harmonic Gen-

eration, and Four-Wave Mixing Microscopy with Single Sub-8 Fs Laser Pulses. *Appl. Phys. Lett.* **2011**, *99* (18), 2−5.
(32) Liu, S.; Vabishchevich, P. P.; Vaskin, A.; Reno, J. L.; Keeler, G. A.; Sinclair, M. B.; Staude, I.; Brener, I. An All-Dielectric Metasurface as a Broadband Optical Frequency Mixer. *Nat. Commun.* **2017**, *9* (1), 1−6.
(33) Rose, A.; Hoang, T. B.; McGuire, F.; Mock, J. J.; Ciracì, C.; Smith, D. R.; Mikkelsen, M. H. Control of Radiative Processes Using Tunable Plasmonic Nanopatch Antennas. *Nano Lett.* **2014**, *14* (8), 4797−4802.
(34) Akselrod, G. M.; Argyropoulos, C.; Hoang, T. B.; Ciracì, C.; Fang, C.; Huang, J.; Smith, D. R.; Mikkelsen, M. H. Probing the Mechanisms of Large Purcell Enhancement in Plasmonic Nanoantennas. *Nat. Photonics* **2014**, *8* (11), 835−840.
(35) Lassiter, J. B.; McGuire, F.; Mock, J. J.; Ciracì, C.; Hill, R. T.; Wiley, B. J.; Chilkoti, A.; Smith, D. R. Plasmonic Waveguide Modes of Film-Coupled Metallic Nanocubes. *Nano Lett.* **2013**, *13* (12), 5866−5872.
(36) Baumberg, J. J.; Aizpurua, J.; Mikkelsen, M. H.; Smith, D. R. Extreme Nanophotonics from Ultrathin Metallic Gaps. *Nat. Mater.* **2019**, *18* (7), 668−678.
(37) Shen, Q.; Boyce, A. M.; Yang, G.; Mikkelsen, M. H. Polarization-Controlled Nanogap Cavity with Dual-Band and Spatially Overlapped Resonances. *ACS Photonics* **2019**, *6* (8), 1916−1921.
(38) Rodriguez, A.; Soljacic, M.; Joannopoulos, J. D.; Johnson, S. G. $\chi^{(2)}$ and $\chi^{(3)}$ Harmonic Generation at a Critical Power in Inhomogeneous Doubly Resonant Cavities. *Opt. Express* **2007**, *15* (12), 7303−7318.
(39) Reuter, G. E. H.; Sondheimer, E. H. Theory of the Anomalous Skin Effect in Metals. *Nature* **1948**, *161*, 394−395.
(40) Boyd, R. W. *Nonlinear Opt.*, 3rd ed.; Academic Press: San Diego, 2008.

https://dx.doi.org/10.1021/acsphotonics.0c00011
ACS Photonics 2020, 7, 901−907